

1 **A conceptual model-based sediment connectivity assessment for patchy agricultural catchments**

2 Pedro V. G. Batista^{1*}, Peter Fiener², Simon Scheper^{1,3}, Christine Alewell¹

3 ¹Department of Environmental Sciences, Universität Basel, Bernoullistrasse 30, 4056, Basel,
4 Switzerland.

5 ²Institute for Geography, Universität Augsburg, Alter Postweg 118, 86159, Augsburg, Germany.

6 ³Dr. Simon Scheper – Research | Consulting | Teaching, Eickhorst 3, 29413 Dähre, Germany

7

8 *Now at Institute for Geography, Universität Augsburg, Alter Postweg 118, 86159, Augsburg,
9 Germany, pedro.batista@geo.uni-augsburg.de

10

11 **Abstract**

12 The accelerated sediment supply from agricultural soils to riverine and lacustrine environments leads to
13 negative off-site consequences. In particular, the sediment connectivity from agricultural land to surface
14 waters is strongly affected by landscape patchiness and the linear structures that separate field parcels
15 (e.g. roads, tracks, hedges, and grass buffer strips). Understanding the interactions between these
16 structures and sediment transfer is therefore crucial for minimising off-site erosion impacts. Although
17 soil erosion models can be used to understand lateral sediment transport patterns, model-based
18 connectivity assessments are hindered by the uncertainty in model structures and input data. In specific,
19 the representation of linear landscape features in numerical soil redistribution models is often
20 compromised by the spatial resolution of the input data and the quality of the process descriptions. Here
21 we adapted the WaTEM/SEDEM model using high resolution spatial data (2 m x 2 m) to analyse the
22 sediment connectivity in a very patchy mesoscale catchment (73 km²) of the Swiss Plateau. We used a
23 global sensitivity analysis to explore model structural assumptions about how linear landscape features
24 (dis)connect the sediment cascade, which allowed us to investigate the uncertainty in the model
25 structure. Furthermore, we compared model simulations of hillslope sediment yields from five sub-
26 catchments to tributary sediment loads, which were calculated with long-term water discharge and
27 suspended sediment measurements. The sensitivity analysis revealed that the assumptions about how
28 the road network (dis)connects the sediment transfer from field blocks to water courses had a much
29 higher impact on modelled sediment yields than the uncertainty in model parameters. Moreover, model
30 simulations showed a higher agreement with tributary sediment loads when the road network was
31 assumed to directly connect sediments from hillslopes to water courses. Our results ultimately illustrate
32 how a high-density road network combined with an effective drainage system increases sediment
33 connectivity from hillslopes to surface waters in agricultural landscapes. This further highlights the
34 importance of considering linear landscape features and model structural uncertainty in soil erosion and
35 sediment connectivity research.

36

37 **1 Introduction**

38 Rainfall events on sloped surfaces continuously displace soil particles, which are transported downslope
39 as sediments. These sediments are then stored and remobilised several times before conceivably
40 reaching surface waters. Accordingly, the sediment cascade is a natural and potentially long
41 geomorphological process (Fryirs, 2013). However, the accelerated sediment supply from agricultural
42 soils to riverine and lacustrine environments leads to negative off-site consequences. Specifically,
43 phosphorus-rich and pollutant-bound particulate matter from arable land is associated to the
44 eutrophication and contamination of water courses (Krasa et al., 2019; Lacey et al., 2021). Extreme
45 erosion events in agricultural fields are also linked to the occurrence of muddy floods (Boardman, 2020)
46 and to damages to downstream infrastructure (Bauer et al., 2019). Therefore, understanding how and
47 when sediment is transferred from agricultural fields to different landscape compartments is imperative
48 to reduce off-site erosion impacts.

49 The degree with which a system facilitates sediment transfer within its internal compartments is defined
50 by Heckmann et al. (2018) as sediment connectivity. This concept can be further distinguished into a
51 structural component, associated to the semi-static spatial configuration of the landscape; and a
52 functional one, which emerges as a dynamic property of the hydro-sedimentological system
53 (Wainwright et al., 2011). Connectivity theory therefore provides a framework to rethink the sediment
54 delivery problem (Fryirs, 2013; Parsons et al., 2009) and to understand the complex spatiotemporal
55 processes that regulate sediment transport.

56 In agricultural landscapes, sediment connectivity is strongly affected by the patchiness of the land use
57 configuration, and the presence of linear features between field parcels (e.g. hedges, grass buffer strips,
58 and roads) (Alder et al., 2015; Bakker et al., 2008; Chartin et al., 2013; Fiener et al., 2011; Remund et
59 al., 2021; Van Oost et al., 2000). The importance of landscape patchiness in regulating sediment transfer
60 is specifically relevant in areas where a large number of small fields, separated by linear structures,
61 create a complex hydrological system. However, the experimental analysis of sediment connectivity at
62 catchment scale is challenging, as it involves measuring both internal soil redistribution processes and
63 cascading sediment transport rates. The interaction between landscape patchiness, linear structures, and
64 sediment connectivity is therefore not addressed by the typical setup of experimental erosion studies,
65 which either focus on small erosion plots or catchment sediment yields (Fiener et al., 2019).

66 Due to the difficulties in measuring the processes that affect sediment movement at catchment and
67 landscape scale, it is common practice to analyse connectivity with modelling approaches (Nunes et al.,
68 2018). These usually rely on high-resolution process-based models, assuming they are able to represent
69 connectivity dynamics (Baartman et al., 2020); semi-qualitative indices (Borselli et al., 2008; Cavalli et
70 al., 2013); or more recently, the coupling of conceptual models with probability theory (Mahoney et al.,
71 2020a, 2020b). In specific, the use of process-based soil erosion and sediment transport models might
72 be an important pathway to improve our understanding of sediment connectivity (Nunes et al., 2018).

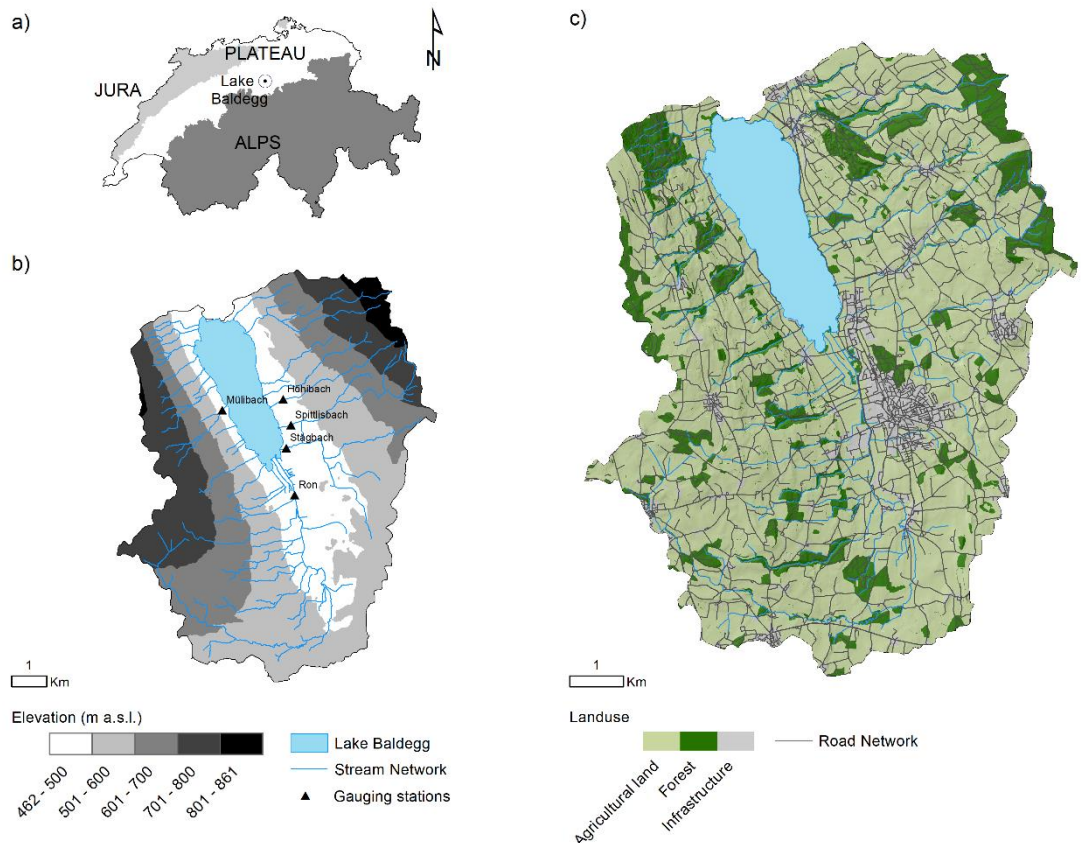
73 However, erosion models in general, and process-based models in particular, face two fundamental
74 problems for representing sediment connectivity : (i) the input data requirements are large and uncertain,
75 and model application is often restricted to small catchments with a maximum size of a few square
76 kilometres (e.g. Baartman et al., 2020; Starkloff and Stolte, 2014; Wilken et al., 2017) and (ii) the
77 implemented process descriptions, especially along linear landscape features and field boundaries, are
78 weakly defined due to the aforementioned unavailability of experimental data. Borrelli et al. (2018)
79 demonstrated how parcel-specific high resolution land cover and management data can improve soil
80 erosion/sediment delivery models in patchy agricultural catchments.

81 Here, we aimed to (i) adapt a conceptual soil erosion and sediment delivery model with high spatial
82 resolution data (2 m x 2 m) within a Monte Carlo framework; (ii) to analyse the sediment connectivity
83 in a very patchy mesoscale catchment (73 km²) in Switzerland; and (iii) to perform a sensitivity analysis
84 of model parameters and structural assumptions regarding how linear features (dis)connect the sediment
85 cascade. Hence, we demonstrate how models can be used to understand the interaction between linear
86 features, landscape patchiness, and sediment connectivity. This will contribute to increase our
87 comprehension of relevant connectivity processes and our ability to develop appropriate measures for
88 reducing off-site erosion impacts.

89 **2 Materials and methods**

90 **2.1 Study catchment**

91 The study catchment consists of the contributing area of the Lake Baldegg, in the central Swiss Plateau
92 (Figure 1). The lake has been extensively studied due to its hypertrophic waters, which have been
93 artificially oxygenated since 1983 (e.g. Lavrieux et al., 2019; Müller et al., 2014; Teranes and
94 Bernasconi, 2005). The eutrophication of the lake has been mostly linked to excessive phosphorus loads
95 during the 20th century (Wehrli et al., 1997). Although water quality in the lake is currently improving
96 (BAFU, 2016), the supply of phosphorus-rich sediment is still a concern to local authorities (von Arb et
97 al., 2021; Stoll et al., 2019). The major advantage of the Baldegg catchment for this study is that a
98 comprehensive hydrological data set is available based on an ongoing, long-term monitoring by the
99 Department of Environment and Energy of the Canton of Lucerne.



100

101 Figure 1. a) Location of the Baldegg catchment; b) elevation, stream network, and location of

102 hydrological gauging stations; c) land use. Data source: Swisstopo (2018, 2020). Sub-catchment areas:

103 Höhibach (2.3 km²), Mülibach (1.6 km²), Stägibach (9.3 km²), Spittlisbach (3.8 km²), Ron (27.7 km²).

104 The Baldegg catchment has a total area of 73.2 km², of which 5.2 km² are covered by the lake. The

105 remaining area is occupied by agricultural land (74%), forests (16%), and infrastructure (e.g.

106 settlements, developed areas, and roads) (10%) (Swisstopo, 2020) (Figure 1c). The agriculture consists

107 of intensively managed pastures and/or meadows, cereal production under crop rotation, permanent

108 grasslands, fruit orchards, and small vineyards (Lavrieux et al., 2019; Stoll et al., 2019). The majority

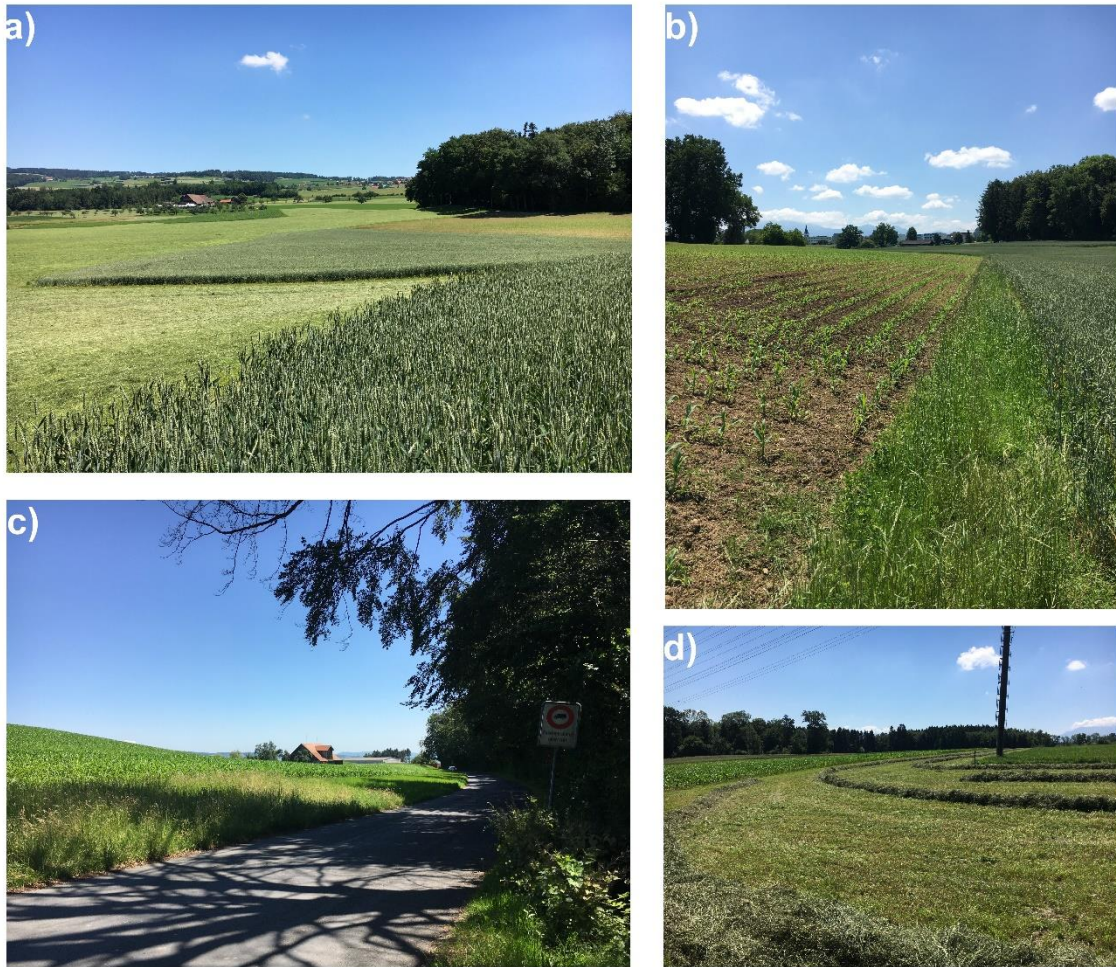
109 of the meadows are composed of a mixture of grasses and clover, which are harvested for silage, hay,

110 or barn feeding up to six times per year (von Arb et al., 2021). Agricultural field blocks, here delimited

111 by external boundaries (e.g. roads, water courses, and forests) (Bircher et al., 2019), have a median size

112 of 4.4 ha. However, smaller patches separated by hedges, tree lines, and grass buffer strips, are generally

113 found within the blocks (Figure 2).



114

115 Figure 2. Typical agricultural landscapes from the Baldegg catchment: a) Small arable and grassland
 116 patches within larger field blocks, b) grass buffer strip between maize and wheat fields, c) wide grass
 117 buffer strip between maize field and a vicinal road, d) freshly cut hay from a pasture between maize
 118 fields.

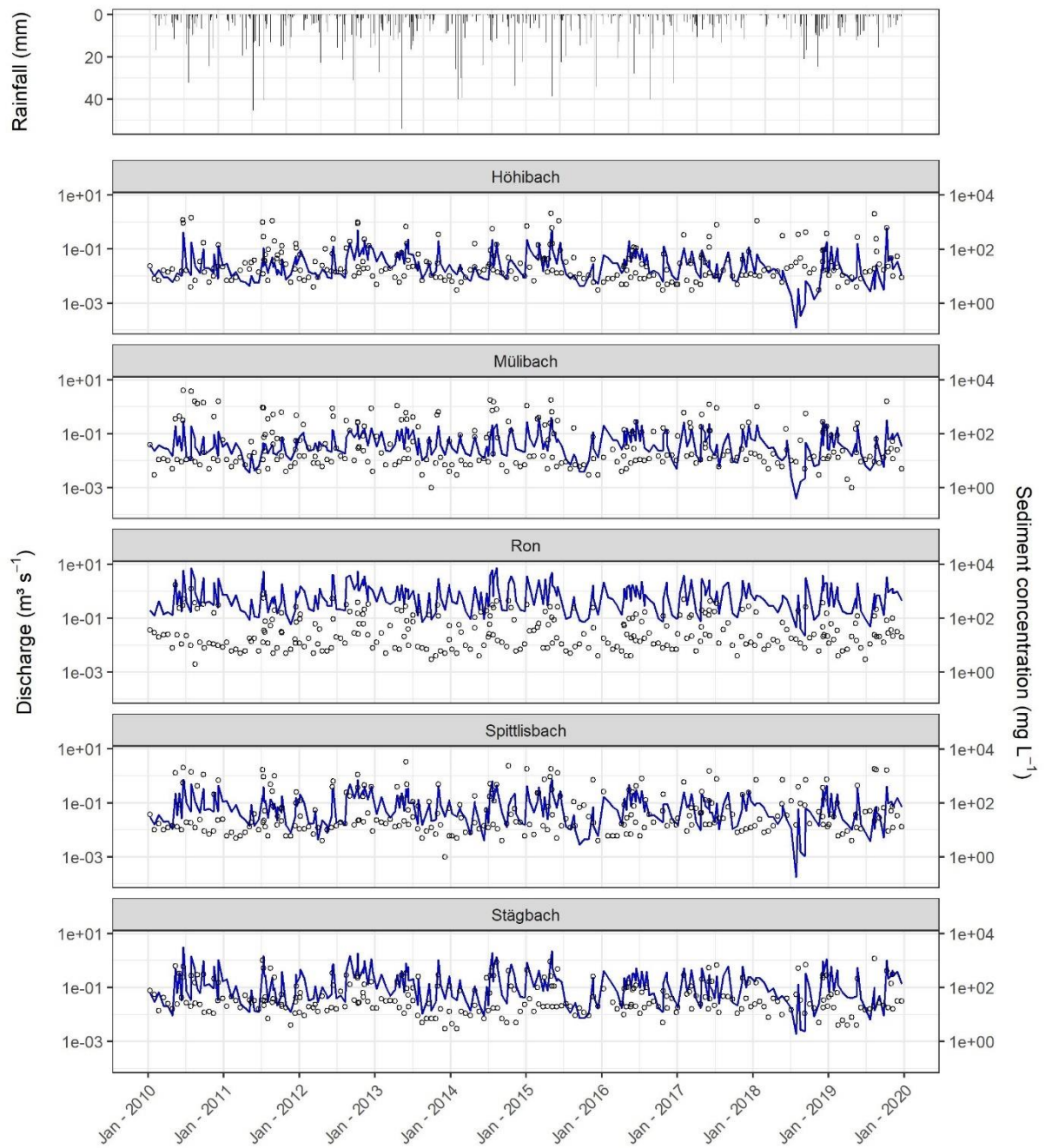
119 The road network density in the Baldegg catchment is 6.0 km km^{-2} , which is approximately three times
 120 higher than the stream density (1.9 km km^{-2}). Streams in the upper catchment are often incised, with
 121 visible, yet not prominent, signs of bank erosion. A total of 22 channels flow into the Lake Baldegg, of
 122 which five streams are monitored for water and sediment discharge by cantonal authorities, as described
 123 in section 2.2.

124 The elevation in the Baldegg catchment ranges from 462 to 861 m a.s.l. Steeper slopes (average values
 125 above 10°) and higher altitudes are found in the eastern and western sides of the catchment (Figure 1b),
 126 in a typical glacial landscape of the Swiss Plateau – in this case formed by the retreat of the Reuss
 127 Glacier in the south to north direction ($\sim 18,000$ years BP) (Keller, 2021; Pfiffner, 2021). As a result,
 128 calcareous Cambisols (IUSS Working Group WRB, 2006) developed upon Tertiary and Quaternary

129 deposits are the main soil class in the catchment. Rainfall is well distributed throughout the year,
130 although greater precipitation is observed from May to August. The average annual rainfall (2010-2019)
131 at the closest gauging station is $\sim 1000 \text{ mm yr}^{-1}$ (Mosen, 454 m a.s.l., $\sim 3.5 \text{ km}$ north of the Lake Baldegg,
132 acquired from MeteoSwiss 2021) and mean rainfall erosivity in the catchment is $\sim 1150 \text{ MJ mm ha}^{-1} \text{ h}^{-1} \text{ yr}^{-1}$ (Schmidt et al., 2016).

134 **2.2 Tributary suspended sediment loads**

135 Suspended sediment concentrations from five tributaries to the Lake Baldegg are monitored by the
136 Department of Environment and Energy of the Canton of Lucerne. Here, we used the data measured
137 from Jan 2010 to Dec 2019. On average 274 grab samples were taken from each tributary, which
138 corresponds to one sample every 22 days, in addition to the samples collected during high-flow events
139 (10 – 13 per year) (Figure 3). Suspended sediments were measured at the same location where water
140 discharge was monitored by automatic gauging stations (Figure 1b). A summary of the measured
141 rainfall, water discharge, and sediment concentration from 2010 to 2019 is displayed in Figure 3.



142

143 Figure 3. Daily rainfall at the Mosen station, mean daily discharge (blue line), and sediment
 144 concentration (circles) at the monitored tributaries of the Lake Baldegg (2010-2019). Data source:
 145 MeteoSwiss (2021).

146 In order to estimate continuous daily sediment concentration values, later used to produce average yearly
 147 sediment loads for each tributary, we used a rating curve approach (Equation 1), combining the roughly
 148 triweekly sediment concentration measurements with continuous discharge measurements. The rating
 149 curve partially accounts for hysteresis and seasonality (Table 1), which can have a significant impact on
 150 sediment export patterns and reflect the catchment landuse, hydrological connectivity, and internal
 151 sediment source dynamics (Sherriff et al., 2016). To derive the coefficients in Equation 1 we used a
 152 parsimonious multivariate regression which does not require separate calibration for different seasons
 153 (Cohn et al., 1992; Vigiak and Bende-Michl, 2013).

154

$$\ln c_i = \beta_0 + \sum_{k=1}^4 \beta_k x_{k,i} + \varepsilon_i \quad (1)$$

155

156 Where: c is sediment concentration (mg L^{-1}) for day i , β_0 is the intercept, β_k are fitted coefficients, $x_{k,i}$
 157 are covariates (Tab. 1) accounting for discharge, hysteresis, and seasonality, k is the covariate
 158 identification, and ε_i is the residual error.

159 Table 1. Covariates used for fitting the sediment-rating curves, as in Vigiak and Bende-Michl (2013).

Covariate	Expression	Explanation	Physical interpretation
$x_{1,k}$	$\ln Q_i$	$Q_i = \text{discharge for day } i \text{ (m}^3\text{s}^{-1}\text{)}$	Discharge
$x_{2,k}$	$(\ln Q_i)^2$	Quadratic term of $x_{1,i}$	Hysteresis
$x_{3,k}$	$\sin(2\pi M_i/12)$	$M_i = \text{month of day } i$	Seasonality
$x_{4,k}$	$\cos(2\pi M_i/12)$	$M_i = \text{month of day } i$	Seasonality

160

161 To analyse the uncertainty in the regressions we simulated posterior distributions of the model
 162 coefficients (β_0, β_k) with an informal Bayesian function of the R package ‘arm’ (Gelman and Hill, 2007),
 163 as in Batista et al. (2021). This function produces realisations of model coefficients based on the residual
 164 standard error of the regression, which means that models with poorer fits will yield broader posterior
 165 distributions of regression coefficients. The posterior distributions were used to simulate 1000 sediment
 166 concentration values for each day i . These were transformed into daily distributions of sediment loads
 167 (Mg), considering the mean daily discharge measurements from the gauging stations. Sediment loads
 168 were ultimately aggregated into average annual values (Mg yr^{-1}) with uncertainty bands, which should
 169 allow for a general comparison with the different sediment connectivity scenarios simulated by
 170 WaTEM/SEDEM.

171 2.3 Model description

172 A modified version of the spatially distributed erosion and sediment transport WaTEM/SEDEM (Van
 173 Oost et al., 2000; Van Rompaey et al., 2001; Verstraeten et al., 2010) was used in this study.
 174 WaTEM/SEDEM provides a framework for modelling sediment connectivity from hillslope to water
 175 courses by use of a steady state transport capacity equation and a pixel-based sediment routing
 176 component. That is, the model assumes that soil particles displaced by water erosion at a given grid cell
 177 are transferred downstream for as long as the runoff transport capacity is greater than the sediment
 178 supply, or until the flow path reaches a definite sink. Although the model is able to simulate both tillage
 179 and water erosion, here we focus on the latter, which is calculated with an adaptation of the RUSLE
 180 (Renard et al., 1997) (Equation 2). We chose to focus on soil erosion by water because in
 181 WaTEM/SEDEM the sediment supply/routing is not affected by tillage erosion. However, tillage
 182 erosion is likely to be an important within-field soil redistribution process in the catchment (please see
 183 the discussion below). The model is by default executed in an average yearly time step, as typical in
 184 RUSLE applications, which predict long-term (~20 years) average annual soil losses:

$$A = R K LS_{2d} C P \quad (2)$$

186
 187 Where: A is average annual soil loss ($\text{kg m}^{-2} \text{yr}^{-1}$), R is rainfall erosivity ($\text{MJ mm m}^{-2} \text{h}^{-1} \text{yr}^{-1}$), K is soil
 188 erodibility ($\text{kg h MJ}^{-1} \text{mm}^{-1}$), LS_{2d} is a topographic factor calculated by the Desmet and Govers (1996)
 189 procedure (dimensionless), C is a cover-management factor (dimensionless), and P is a support practice
 190 factor (dimensionless).

191 Transport capacity ($\text{kg m}^{-1} \text{yr}^{-1}$) per unit widths of grid cells is assumed to be proportional to the potential
 192 to rill erosion, which is described by a power function of slope length and gradient (Van Rompaey et
 193 al., 2001):

$$TC = K_{TC} RK (LS_{2d} - 4.12 S_g^{0.8}) \quad (3)$$

195
 196 Where: K_{TC} is a landuse-dependent transport capacity coefficient (m) which requires calibration, R is
 197 rainfall erosivity ($\text{MJ mm h}^{-1} \text{yr}^{-1}$), K is soil erodibility ($\text{t h MJ}^{-1} \text{mm}^{-1}$), LS_{2d} is a topographic factor
 198 calculated by the Desmet and Govers (1996) procedure (dimensionless), and S_g is slope gradient (m m^{-1}).
 199

200 WaTEM/SEDEM partially incorporates the influence of the landscape structure on sediment transfer by
 201 the use of a parcel connectivity parameter P_{Con} , which represents the proportion of sediment that is
 202 stopped at field borders. The model also simulates runoff connectivity by means of a parcel trapping
 203 efficiency P_{TEf} parameter, which corresponds to the proportion of the flow accumulation that is routed

204 downstream. Finally, the model is able to estimate the total amount of sediment transferred from
205 hillslopes to water courses, which can be interpreted as the hillslope component of a catchment sediment
206 budget. Since WaTEM/SEDEM does not represent gully and bank erosion, nor in-stream erosion and
207 deposition processes, any comparison between modelled sediment yields and catchment-outlet sediment
208 loads must be interpreted with caution. However, in catchments where rill and interrill are the main
209 overland erosion processes, and assuming a state of long term fluvial quasi equilibrium, the outlet
210 sediment loads should be at least comparable to the model outputs – even if not fully commensurable.
211 For further information on the model, we refer to Notebaert et al., (2006), Van Oost et al., (2000), Van
212 Rompaey et al., (2001), and Verstraeten et al., (2010).

213 **2.4 Model implementation, input data, and sensitivity analysis**

214 WaTEM/SEDEM is implemented as a user-friendly GUI developed at KU Leuven (Notebaert et al.,
215 2006). Although the software facilitates model application, it does not allow for more complex
216 operations, such as sensitivity or uncertainty analysis. Moreover, some model components might not be
217 fully comprehensible without access to the source code, and WaTEM/SEDEM is frequently used as a
218 black box. Hence, in order to perform a sensitivity analysis of model parameters and underlying
219 structural model assumptions, we implemented a WaTEM/SEDEM version using the free open source
220 software R (R Core Team, 2021) and SAGA GIS (Conrad et al., 2015). The main adaptations are
221 described in the following, and our code is available as supplementary material.

222 Our model application consists of a global all-at-a-time sensitivity analysis, as described by Pianosi et
223 al. (2016). That is, we performed a Monte Carlo simulation to explore the variability of the whole
224 parameter space, and all input factors were sampled simultaneously for each model realisation ($n =$
225 1200). The framework is similar to an uncertainty analysis, except in this case we did not focus on
226 locating the parameter space which produced behavioural model realisations. Instead, we concentrated
227 on apportioning sources of uncertainty to different model input factors, aiming to rank their contribution
228 to the variability of the response surface (see Pianosi et al., 2016 for a review on sensitivity analysis).
229 This should allow us to identify parameters and model assumptions that have a greater impact on the
230 manner with which WaTEM/SEDEM describes sediment connectivity in the Baldegg catchment. In
231 particular, the analysis of different assumptions about the structure of the model should provide a
232 connectivity assessment based on the quantification of the structural uncertainty within the simulations.
233 To the best of our knowledge, this is the first time the analysis of model structural error is incorporated
234 to sediment connectivity research.

235 For each iteration of the Monte Carlo simulation, RUSLE input variables were sampled from uniform
236 distributions (Table 2). Minimum and maximum R factor values were retrieved from the Swiss national
237 map (Schmidt et al., 2016), and a single lumped value for the whole catchment was sampled for each
238 iteration. The same approach was used for the K factor (Schmidt et al., 2018a). We used lumped
239 catchment values for these factors due to their low spatial variability within the study area, according to

240 the national maps (coefficient of variations are 1% and 7% for the K and R factor, respectively). For the
241 C and P factors, here combined in a single CP parameter, uniform distributions were created for each
242 landuse class in the catchment, based on commonly used values from the literature and a land cover map
243 (1:25000) (Swiss Map Vector 25 BETA) (Swisstopo, 2018), which we rasterised to the model resolution
244 (2 m x 2 m). Due to the difficulties involved in accurately representing long-term average agricultural
245 landuse patterns and farming management practices per field parcel, pastures and cropland were
246 considered a single arable land category, using only the information available from the land cover map
247 (Table 2) (Swiss Map Vector 25 BETA) (Swisstopo, 2018). In this case, minimum and maximum values
248 were relaxed to represent a wide possible combination of crops and support practices. Such
249 combinations were assessed with the CP -Tool (Kupferschmied, 2019), which allows for the calculation
250 of CP values considering common crop rotation systems in Switzerland. The minimum CP values were
251 particularly reduced to include typical values for permanent grasslands in Switzerland (~0.01) (Schmidt
252 et al., 2018b). This simplified approach should be appropriate considering i) our focus on connectivity
253 scenarios and linear landscape structures, and ii) the use of the Monte Carlo simulation with the sampling
254 of a wide parameter space that accounts for the uncertainty in the landuse classification. Finally, the LS_{2d}
255 factor was calculated with a slope (rad) and an upslope contributing area (m^2) grid, which were obtained
256 by processing a 2 m x 2 m resolution DEM from SwissALTI3D (Swisstopo, 2014a). In this case, the
257 error in the LS_{2d} factor was not incorporated into Monte Carlo simulation due to the use of the high-
258 resolution DEM, which should considerably reduce the uncertainty associated to the parameter
259 estimation.

260 Table 2. Minimum and maximum parameter values sampled during the Monte Carlo simulation.

Parameter	Category	Min	Max
R (MJ mm m ⁻² h ⁻¹ yr ⁻¹)		950 10 ⁻⁴	1350 10 ⁻⁴
K (kg h MJ ⁻¹ mm ⁻¹)		0.025 10 ³	0.040 10 ³
CP (-)	Arable land	0.01	0.5
	Grass buffer strips	0.001	0.009
	Forest	0.0001	0.003
	Orchard	0.001	0.2
	Vineyard	0.05	0.6
K_{TC} (m)	High (arable land, vineyard)	1	200
	Low (grass buffer strips, forest, orchard)	1	100
P_{TEf} (-)		0	1
P_{Con} (-)		0	1

261

262 Similarly, all WaTEM/SEDEM-specific model parameters were sampled from uniform distributions
 263 (Table 2). Landuse classes with a CP factor above 0.01 received higher transport capacity coefficients
 264 (K_{TC} high). The remaining landuse classes, namely forests and grass strips, received lower coefficients
 265 (K_{TC} low). The K_{TC} reference values were taken from Van Rompaey et al. (2001) and extended in order
 266 to explore a larger parameter space. The sampled parcel trapping efficiency (P_{TEf}) values were assigned
 267 to forests and grass buffer strips in the rasterised land cover map, as we explain below. The resulting
 268 P_{TEf} grid was used as a weight for calculating the aforementioned upslope contributing area. Hence, only
 269 a proportion of the grid-cell area from forests and grass strips contributed to the downstream flow
 270 accumulation, as runoff amounts are assumed not to increase (or to increase slowly) with slope length
 271 under natural vegetation (Govers, 2011). Parcel connectivity (P_{Con}) values were assigned to the forest
 272 and grass buffer strips cells that bordered agricultural fields, representing the extent with which water
 273 and sediment transport is reduced at parcel borders (Notebaert et al., 2006). The transport capacity (Eq.
 274 2) at these cells was reduced by a fraction inversely proportional to the sampled P_{Con} value.

275 For each sampled combination of parameters values, the models were applied with and without the
 276 presence of grass buffer strips between agricultural field blocks and adjacent roads and forests. Although
 277 grass buffer strips are generally present at field borders in the Baldegg catchment (Figure 2), these
 278 features were not distinguishable in the land cover map. Hence, we manually inserted 2 m wide grass
 279 buffer strips at the aforementioned borders. The extent of the buffer-strips in reality is quite variable,
 280 and generally wider at forest and river vicinities (3 – 6 m), as required by law in Switzerland (Alder et
 281 al., 2015). For simplicity, we used a single value that should allow us to test the sensitivity of the model
 282 to the presence of the strips. The 2 m width was selected based on the spatial resolution of the model
 283 input data. Hedges and tree lines within field blocks were already classified in the large-scale
 284 topographic landscape model of Switzerland (swissTLM3D) (Swisstopo, 2020) and required no
 285 additional processing apart from a merge with the land cover map (Swiss Map Vector 25 BETA)
 286 (Swisstopo, 2018).

287 Furthermore, three road connectivity assumptions were assessed for each model iteration. For such, we
288 first converted the roads from polylines (as available in the swissTLM3D) to polygons, using a buffer
289 distance based on the road widths. Next, these polygons were rasterised and incorporated into the land
290 cover grid used for modelling. In a first scenario, roads were treated as an ultimate sink, with zero
291 transport capacity (i.e., ‘roads as sinks’). Hence, sediments reaching roads or infrastructure were
292 subsequently removed from the system and did not reach surface waters. This represents a scenario in
293 which roadside ditches and the road drainage system trap most sediments and partly diverge runoff to
294 wastewater treatment plants. A second scenario assumed that all sediments reaching the road network
295 were directly connected to the stream network. This represents a situation in which the road drainage
296 system acts as a hydraulic shortcut, transferring sediments from fields into surface waters (i.e., ‘roads
297 as shortcuts’) (see Schönenberger and Stamm, 2021). As in the original model formulations (see
298 Notebaert et al., 2006), the third scenario assigned very high transport capacity to roads and
299 infrastructure, so that no deposition would take place (i.e. ‘roads as patch connectors’). In this case,
300 runoff and sediment might flow along or across the road network – which is expected to happen during
301 extreme rainfall events when the drainage system is clogged. For this scenario, deposition will never
302 occur on road cells, however sediments can still be deposited on lower patches before reaching the
303 stream network. Hence, sediment transfer will be entirely dependent on the flow direction calculated
304 from the DEM. Here we employed a multiple flow direction algorithm, which was used for calculating
305 upslope contributing area and routing sediments along the flow path. The sediment routing component
306 was implemented with a capacity accumulation function from SAGA GIS (Conrad et al., 2015), and all
307 geo-processing tools were applied with the ‘RSAGA’ package (Brenning et al., 2018).

308 The sensitivity of WaTEM/SEDEM to the uncertainty in model parameters, the presence of grass buffer
309 strips, and assumptions about road connectivity (i.e., model structural uncertainty) was assessed by
310 evaluating modelled hillslope sediment yields (i.e., the amount of sediment delivered from hillslopes to
311 surface waters) for the entire Baldegg catchment. A qualitative analysis was performed with a visual
312 inspection of scatter plots, comparing the univariate parameter space with the model response surface.
313 Additionally, we used a random forest analysis (RFA) to rank the importance of input factors to the
314 uncertainty in model outputs (Antoniadis et al., 2021). That is, a random forest was used to predict the
315 WaTEM/SEDEM-modelled sediment yields, based on the sampled parameter values for each iteration
316 of the Monte Carlo simulation. The importance of the input factors, including model parameters, the
317 presence of grass strips, and the road connectivity scenarios, was ranked based on their relative
318 contribution to the RFA predictive error, following an out-of-bag estimate (Breiman, 2001). We chose
319 the RFA due to its ability to rank both qualitative and quantitative input factors. The analysis was
320 performed with the ‘randomForest’ (Liaw and Wiener, 2002) R package.

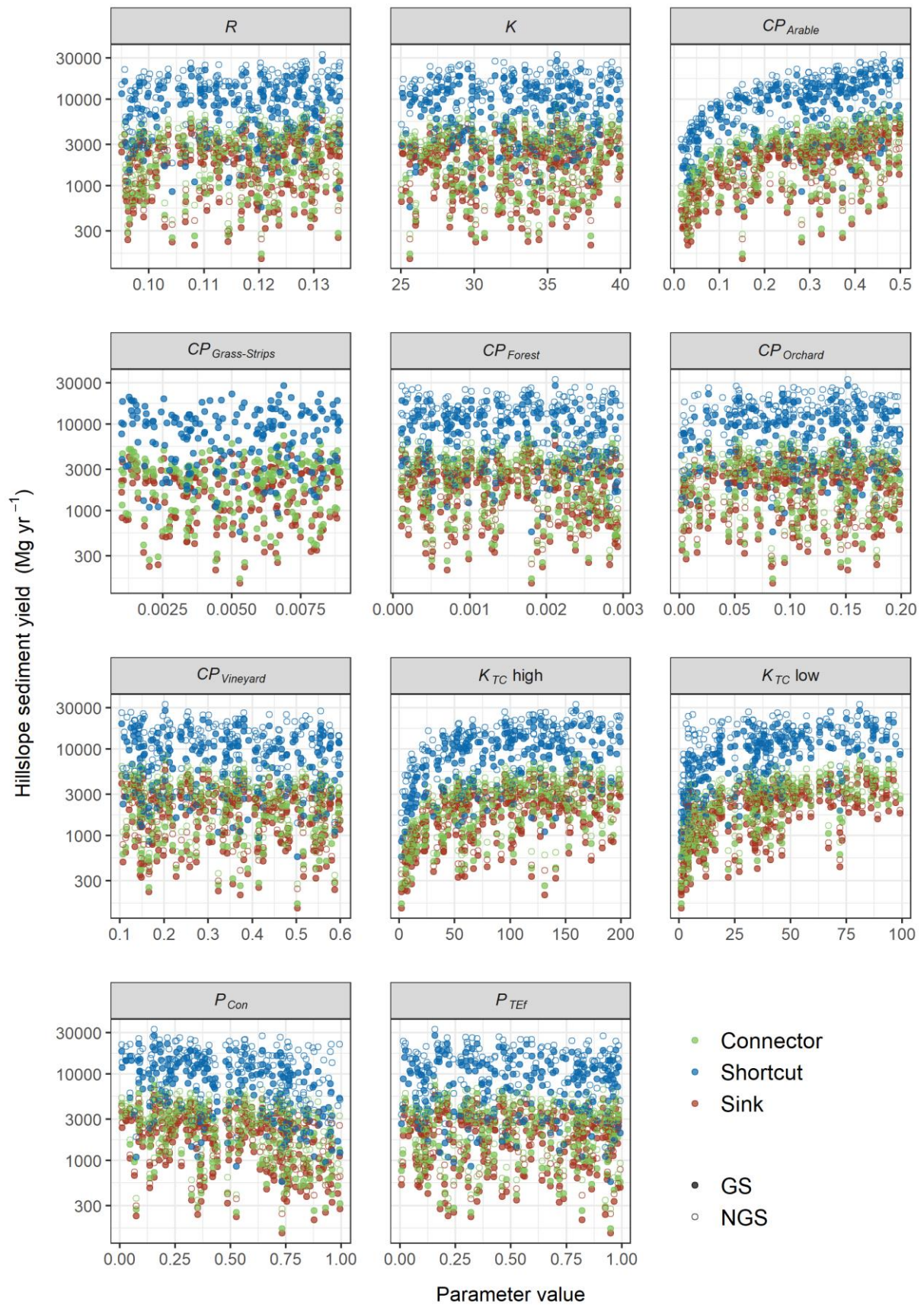
321 Finally, we compared the resulting WaTEM/SEDEM simulations of sub-catchment hillslope sediment
322 yields to the suspended sediment loads from the monitored tributaries. Of note, with this comparison we

323 only aim to provide a general picture of the plausibility of the model realisations. Suspended sediment
324 loads are a product of a complex interaction of hillslope and channel remobilisation processes, which
325 are not fully represented by WaTEM/SEDEM. In addition, since the model is RUSLE-based, the soil
326 redistribution rates represent long-term average annual values, which hampers a straightforward
327 comparison with annual sediment transport rates. Hence, modelled hillslope yields and suspended loads
328 are not entirely commensurable, and we did not focus on a rejectionist framework for model testing.
329 This research is exploratory and investigates the importance of linear features and landscape patchiness
330 on sediment connectivity.

331 **3 Results**

332 **3.1 Sensitivity analysis**

333 The road connectivity assumptions were by far the most sensitive input factor for WaTEM/SEDEM in
334 the Baldegg catchment. This is illustrated in Figure 4, which presents scatter plots comparing sampled
335 parameter values and the model response surface. The uniformly scattered points denote a low
336 sensitivity of the modelled hillslope sediment yields to most input factors, with some evident exceptions:
337 CP for arable land, K_{TC} high, and K_{TC} low. On the other hand, all plots demonstrate that higher sediment
338 yields were calculated when we assumed that roads behaved as hydraulic shortcuts, directly connecting
339 agricultural patches to the stream network.

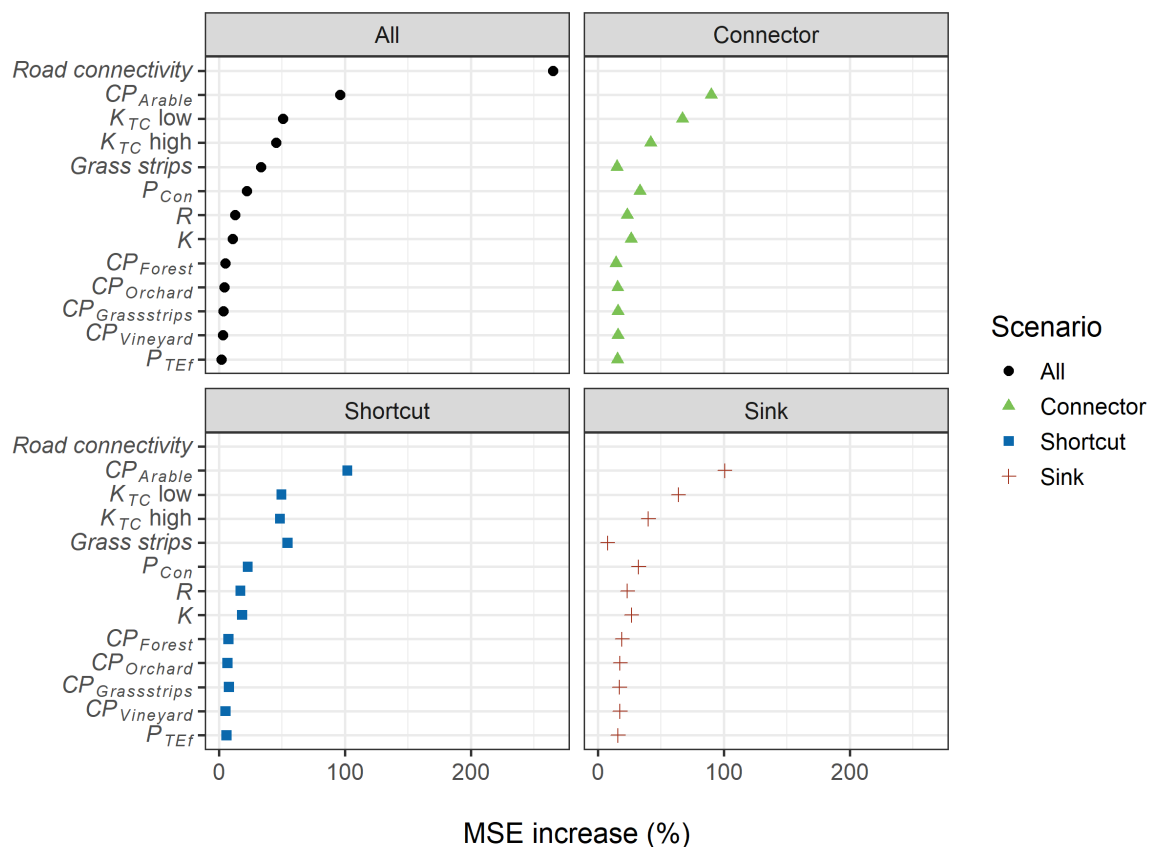


340

341 Figure 4. Univariate scatter plots of sampled parameter values. Full circles represent model realisations
 342 with the presence of grass buffer strips (GS), and open circles represent the ones without strips (NGS).

343 Colours represent the road connectivity assumptions (i.e. 'roads as patch connectors', 'roads as hydraulic
344 shortcuts', and 'roads as sinks'). See section 2.4 for a description of road connectivity scenarios.

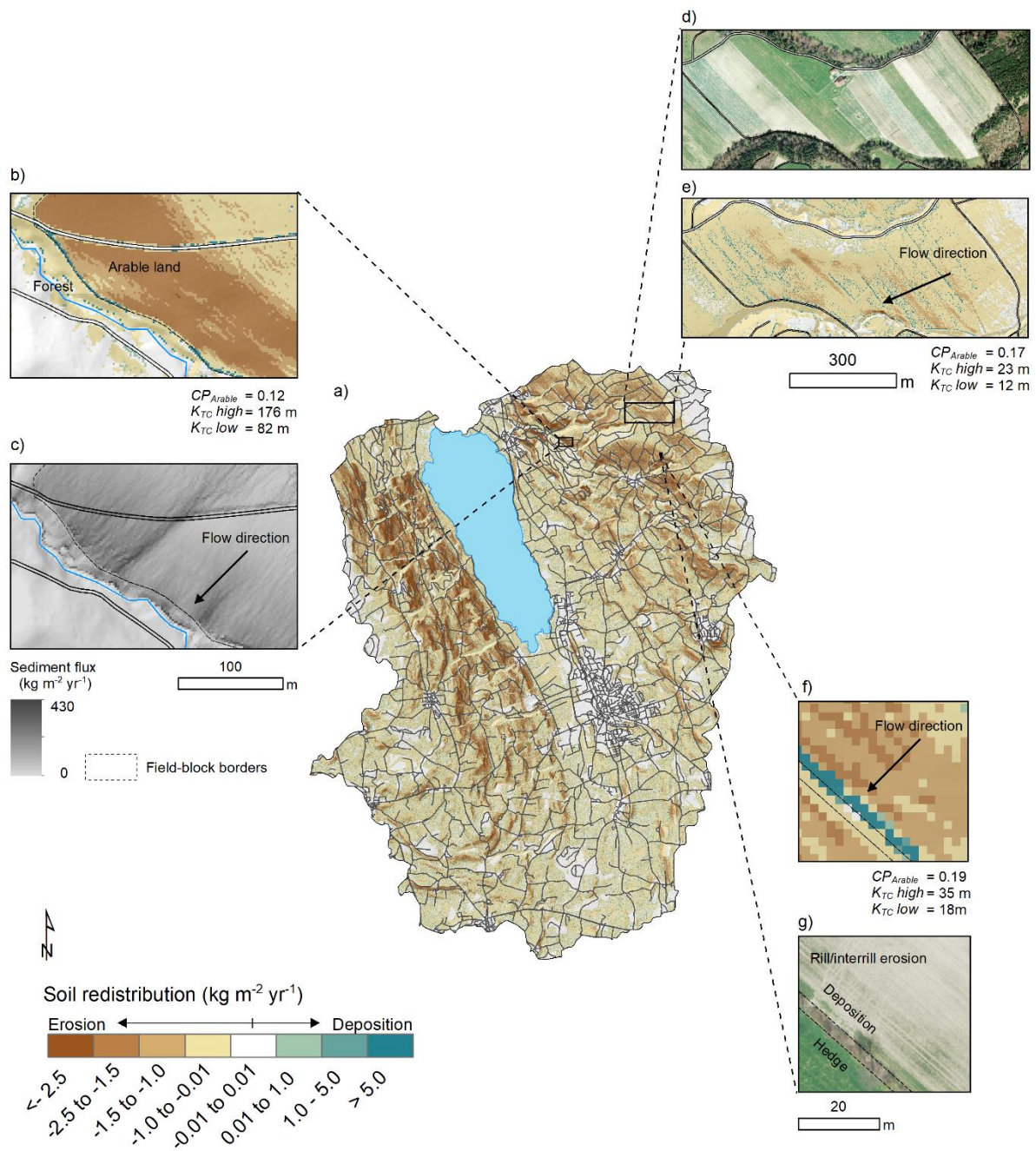
345 Similarly, the results from the RFA demonstrate that road connectivity was the most important input
 346 factor for predicting the WaTEM/SEDEM outputs (Figure 5). That is, if road connectivity was not
 347 considered, the predictive mean squared error (MSE) of the RFA increased by 265%. The MSE increase
 348 associated to CP for arable land (96%), K_{TC} low (51%), K_{TC} high (45%), and the presence of grass buffer
 349 strips (33%), indicate the model was also sensitive these input factors. However, if we considered each
 350 road connectivity scenario individually, the results from the random forest were shifted, as the model
 351 seemed to be more sensitive to the presence of grass buffer strips for the ‘road as shortcuts’ scenario
 352 (MSE increase = 55%).



353
 354 Figure 5. Mean squared error (MSE) increase associated to model input factors for the Random Forest
 355 Analysis (RFA). Larger relative errors indicate the input factors were more important for estimating
 356 model outputs.

357 3.2 Spatial patterns

358 The spatial patterns of soil redistribution rates were also highly influenced by linear features, landscape
 359 patchiness, and connectivity assumptions. Sediment deposition on field blocks downslope from roads
 360 was more frequently observed for the ‘roads as connectors’ scenario, than for the other road connectivity
 361 assumptions. Specifically, when sediments were not diverged or trapped by the road network, there was
 362 a greater proportion of sediment deposition on footslope field borders and other potential sinks (Figure
 363 6b) (Table 3).



365

366 Figure 6. a) Catchment patterns of soil redistribution for a model realisation with the presence of grass
 367 buffer strips; b) detail of sediment deposition on field borders, 'road as patch connectors' scenario; c)
 368 detail of sediment fluxes across the road network, 'road as patch connectors' scenario'; d) detail of aerial
 369 image of multiple parcels within a field block (Swisstopo, 2014b); e) soil redistribution rates for the
 370 field block; f) detail of sediment deposition at a grass buffer strip at a field border; g) aerial image for
 371 the field (Swisstopo, 2014b).

372

373 The sediment flux from agricultural fields was generally interrupted when entering forest patches, and
 374 further deposition was modelled at forested valley floors, near the stream channels, for all scenarios
 375 (Figure 6b, c). Importantly, sediment deposition along grass buffer strips, hedges, and tree lines reduced
 376 sediment fluxes in between field blocks, forming a patchy connectivity pattern. This was again visible
 377 for all simulated connectivity assumptions, albeit particularly pronounced when the presence of grass
 378 buffer strips was considered (Figure 6 a, f).

379 Unexpectedly, the soil redistribution patterns revealed that WaTEM/SEDEM simulated linear
 380 deposition areas at the borders of small cropland patches (Figure 6d, e). This occurred even in the
 381 absence of grass buffer strips or hedges, and hence without P_{Con} parameterisation, which was only
 382 applied to field-block borders. These depositional patterns were particularly evident within field blocks
 383 oriented across the slope direction, and apparently stem from small scale changes in the slope gradient,
 384 which were represented by the high-resolution DEM and which potentially results from long-term tillage
 385 erosion.

386 3.3 Soil redistribution rates, hillslope sediment-yields, and suspended sediment loads

387 Soil redistribution rates for eroding grid cells in the Baldegg catchment were almost identical among the
 388 simulated road connectivity assumptions (Table 3). Higher absolute deposition rates were calculated for
 389 the simulations without grass strips for both the connector and sink scenarios, which is a result of
 390 increased erosion rates calculated without the presence of the strips. On the other hand, lower sediment
 391 yields were calculated with the presence of grass buffer strips when the connectivity scenarios were
 392 analysed individually. Among these scenarios, deposition rates were lower if roads were considered to
 393 behave as hydraulic shortcuts. Contrarily, deposition rates for the ‘roads as connectors’ and ‘roads as
 394 sinks’ scenarios were very similar, although road deposition was only modelled in the second case.
 395 Therefore, deposition rates within fields, patch borders, colluviums, and valley floors for the connector
 396 scenario were ~30% higher than for the other simulations. As the sediments not diverged by the road
 397 network were ultimately deposited within the catchment, the sink and connector scenarios displayed
 398 very similar hillslope sediment yields. Contrarily, sediment yields for the shortcut scenario were in
 399 general ~4.5 times higher than for the remaining road connectivity simulations.

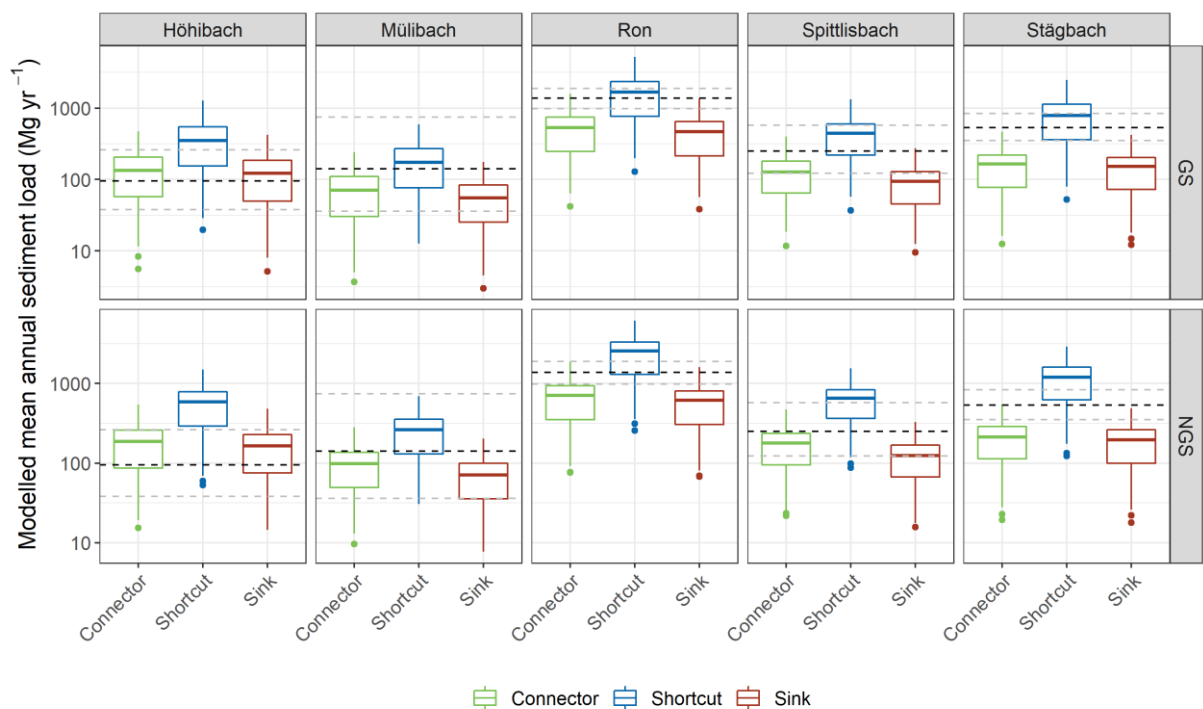
400 Table 3. Summary statistics of soil redistribution rates, hillslope sediment yields calculated by the
 401 WaTEM/SEDEM simulations.

Scenario		Erosion			Deposition			SSY			SY		
		----- Mg ha ⁻¹ yr ⁻¹ -----									----- Mg yr ⁻¹ -----		
		Q1	Q2	Q3	Q1	Q2	Q3	Q1	Q2	Q3	Q1	Q2	Q3
Connector	GS	3.5	6.3	8.7	3.4	5.9	8.3	0.2	0.3	0.5	1,047	2,248	3,307
	NGS	3.7	6.6	9.1	3.5	6.1	8.5	0.2	0.4	0.6	1,498	3,054	4,097
Shortcut	GS	3.5	6.3	8.8	2.7	4.9	7.2	0.6	1.2	1.8	3,878	8,467	12,242
	NGS	3.7	6.6	9.2	2.5	4.7	6.7	0.9	1.9	2.6	6,303	13,238	17,506

Sink	GS	3.5	6.3	8.8	3.4	6.0	8.4	0.1	0.3	0.4	833	1,828	2,665
	NGS	3.7	6.6	9.2	3.5	6.2	8.7	0.2	0.4	0.5	1,143	2,389	3,197

402 SSY: area specific hillslope sediment yield; SY: hillslope sediment yield. Deposition rates include
 403 hillslope and road deposition. GS: grass buffer strips; NGS: no grass buffer strips; Q1: first quartile, or
 404 the 25th percentile; Q2: second quartile, or the median; Q3: third quartile, or the 75th percentile.

405 The comparison between WaTEM/SEDEM simulations and the tributary sediment loads revealed a
 406 larger overlap between the latter and the results from the ‘road as shortcuts’ scenario (Figure 7). The
 407 overlap became particularly clear when we compared the prediction intervals of the calculations (Figure
 408 7). That is, a smaller proportion of the ‘road as connectors’ and the ‘road as sinks’ model realisations
 409 encompassed the tributary sediment loads, except for the Höhibach, which showed the opposite pattern.
 410 This behaviour was particularly evident for the scenario with the presence of grass buffer strips.



411
 412 Figure 7. Box-plots of hillslope sediment loads simulated by WaTEM/SEDEM for the road connectivity
 413 scenarios for each tributary sub-catchment. Dashed lines represent the median (in black) and the 95%
 414 interval (in grey) of the measurement-based estimates of sediment loads for each tributary, calculated
 415 from the error propagation of the sediment-rating curve. GS: grass buffer strips, NGS: no grass buffer
 416 strips. Simulations for the shortcut scenario generally shows a higher overlap with calculated sediment
 417 loads, in particular when grass buffer strips are considered.

418 It is important to note that the median daily sediment concentrations calculated from the 1000
 419 realisations of the rating curves (Equation 1) underestimated the high sediment concentration
 420 measurements, for all tributaries. This resulted in the positive mean error of the median estimates (Table
 421 4). Moreover, the Nash-Sutcliffe model efficiency coefficient for the median calculations was
 422 unsatisfactory considering the usual thresholds for model performance (e.g. Moriasi et al., 2015).

423 However, the 95 % prediction interval of the rating curves encompassed a large proportion of the
 424 sediment concentration observations for the tributaries with poorer fits and wider uncertainty bands (i.e.,
 425 the Höhibach, Mülibach, and Spittlisbach) (Table 4, Supplementary Material Figure 1). The sediment
 426 rating curves for the tributaries which displayed a better fit (i.e., the Ron and Stägbach) encompassed a
 427 much lesser proportion of the observed sediment concentration values (Table 4, Supplementary Material
 428 Figure 1). That is, the regressions with the lowest residual standard errors had narrower uncertainty
 429 bands, which albeit produced more accurate median predictions, led to a greater proportion of
 430 observations out-of-bound from the 95 % prediction interval. In any case, the largest errors were
 431 associated to underestimates of extreme events, and therefore, it is likely that actual sediment loads from
 432 the tributaries are contained within the long right side of the skewed distributions resulting from the
 433 error propagation of the rating curves (Figure 7), which would increase the overlap with the shortcut
 434 scenario.

435 Table 4. Evaluation metrics of the sediment rating curve, considering the measured sediment
 436 concentrations and median of the simulations.

Stream	ME ----- mg L ⁻¹ -----	RSME	Out-of-bound percentage* ----- % -----	r _p	r _s	NSE
Höhibach	56.58	80.51	13	0.51	0.61	0.20
Mülibach	96.17	142.96	14	0.56	0.72	0.24
Ron	24.18	55.42	75	0.62	0.76	0.35
Spittlisbach	108.84	155.85	29	0.46	0.63	0.14
Stägbach	33.88	68.46	51	0.47	0.68	0.15

437 *percentage of observations out of the 95 % prediction interval. ME: mean error; RMSE: root-mean-
 438 square error, r_p: Pearson's correlation coefficient, r_s: Spearman's correlation coefficient; NSE: Nash-
 439 Sutcliffe model efficiency coefficient.

440 **4 Discussion**

441 Here we assessed the interaction between landscape patchiness, linear structures, and sediment
 442 connectivity. Our quantitative model-based approach highlighted the importance of roads in
 443 (dis)connecting sediment fluxes between landscape compartments and surface waters in patchy
 444 agricultural catchments. These findings are in lines with long-term field observations and qualitative
 445 model assessments for similar areas in Switzerland.

446 For instance, Ledermann et al. (2010) monitored off-site erosion in multiple fields from different regions
 447 of the Swiss midlands and found that linear features in general and roads in particular had a large
 448 influence on runoff concentration, soil erosion rates, and off-site damage. These authors also estimated
 449 that > 50 % of eroded soil was deposited in adjacent fields and infra-structure, while up to 20 % reached
 450 surface waters, mainly through indirect inflow via the road and drainage network. Such figures are
 451 proportionate to WaTEM/SEDEM simulations for the Baldegg catchment, specifically for the shortcut

452 scenario with the presence of grass buffer strips (Table 3). Another interesting similarity between our
453 outputs and the field assessments from Ledermann et al. (2010), was that both approaches identified
454 field border structures as critical regulators of soil erosion and sediment transport (see Figures 5 and 6).
455 According to the field assessments, border furrows are specifically important for both triggering erosion
456 and promoting diffuse sediment deposition. Such features, combined with long-term tillage erosion,
457 might be responsible creating the topographic pattern displayed in Figure 6d.

458 Moreover, the capacity of roads to connect runoff and sediments from arable land to surface waters in
459 Switzerland was extensively described by Alder et al. (2015) and Schönenberger and Stamm (2021).
460 Both studies used a similar semi-qualitative modelling approach for identifying agricultural fields that
461 were directly or indirectly (i.e. via the road and drainage networks) connected to surface waters. In
462 particular, Schönenberger and Stamm (2021) mapped the location of drainage inlets in multiple small
463 catchments of the Swiss Plateau. Accordingly, these authors identified the road drainage system as the
464 main hydraulic shortcut connecting fields to water courses, as most drainage inlets discharge into surface
465 waters (87%), and only a small proportion of them flow into wastewater treatment plants or depositional
466 areas. Hence, the fact that the WaTEM/SEDEM ‘road as shortcuts’ scenario displayed a greater
467 agreement with the sediment rating curves for the Baldegg tributaries (Figure 7) is coherent with the
468 current understanding of runoff dynamics in the Swiss Plateau. Of note, the contrasting results for the
469 Höhibach sediment loads (Figure 7), which are much closer to the sink and patch-connector simulations,
470 do not seem to be explained by any physiographical characteristic of the sub-catchment (Supplementary
471 Material Table 1). Hence, we speculate that this different pattern could be caused by a lower inlet
472 drainage density or specific farming practices within the Höhibach contributing area.

473 In addition, our simulations of edge-of-field grass buffer strips indicated that these structures might be
474 particularly relevant for the ‘road as shortcuts’ scenario. In this case, the model estimated that grass trips
475 could reduce up to 30% the sediment connectivity from hillslopes to surface waters in the Baldegg
476 catchment (Table 4). However, we assumed 2 m wide strips at field block borders, irrespectively of the
477 adjacent structures or land use. As previously mentioned, the extent of these features is in fact quite
478 variable, and legislation only requires 0.5 m filters between fields and roads, as reported by Alder et al.
479 (2015). These authors further emphasised that albeit edge-of-field strips are an important
480 complementary management practice, their effectiveness is often reduced in case of large drainage areas,
481 in which very wide buffers would be necessary to stop sediment fluxes. Hence, Alder et al. (2015)
482 recommended that minimising on-site erosion rates was ultimately the most effective way to decrease
483 sediment input from arable land to water courses in Switzerland. Our results support this management
484 proposition. However, our simulations also indicate that the disproportional sediment connectivity
485 afforded by the dense road network translates into an excessive sediment supply to water courses, even
486 when simulated erosion rates were small. As on-site erosion rates in Switzerland are already reasonably
487 low (see Prasuhn, 2020), it might be important to consider solutions that address the sediment transport

488 through the underground drainage system, particularly in environmentally sensitive areas, such as the
489 Baldegg catchment.

490 In a wider context, our study has demonstrated how structural sediment connectivity patterns can be
491 investigated with a conceptual model such as WaTEM/SEDEM, provided that model spatial resolution
492 is sufficiently fine to represent relevant features and processes. In agricultural catchments of the Swiss
493 Plateau and likely in other patchy landscapes, soil redistribution rates and patterns are intrinsically linked
494 to linear features (see Alder et al., 2015; Ledermann et al., 2010; Prasuhn, 2020; Remund et al., 2021).
495 Hence, in order to provide relevant system descriptions, soil erosion models applied under similar
496 conditions must be able to represent linear features and landscape patchiness. Although our results might
497 seem case-specific, similar findings have been reported around the world. For instance, the effects of
498 roads and farm tracks in both coupling and decoupling runoff and sediments has been described in
499 Australia (Croke et al., 2005), Brazil (Bispo et al., 2020), Kenya (Stenfert Kroese et al., 2020), Italy
500 (Persichillo et al., 2018), Spain (Calsamiglia et al., 2018), and the USA (Mahoney et al., 2018).
501 Moreover, the influence of linear features such as field borders, hedges, terraces, and tractor tram lines
502 on soil redistribution rates have been well documented in Europe (Calsamiglia et al., 2018b; Evrard et
503 al., 2009; Fiener and Auerswald, 2005; Lacoste et al., 2014; Saggau et al., 2019), as well as the
504 importance of landscape structure in regulating sediment connectivity (Baartman et al., 2020; Chartin et
505 al., 2013; Fiener et al., 2011).

506 Another generalisable finding from our research was that WaTEM/SEDEM can be as sensitive to
507 RUSLE parameters as to the model-specific transport capacity coefficients. Therefore, when performing
508 uncertainty analyses of WaTEM/SEDEM, it is important to consider sources of error associated to the
509 RUSLE parameterisation. So far, uncertainty estimation methods applied to WaTEM/SEDEM have
510 focused on the K_{TC} parameterisation, and therefore have underestimated the uncertainty in model
511 predictions. We anticipate that our open-source WaTEM/SEDEM script will facilitate stochastic
512 implementations of the model, and ultimately promote uncertainty and sensitivity analysis of soil erosion
513 models. In particular, the open-source code will allow model users to explore structural uncertainties,
514 which can contribute to increase our understanding of sediment connectivity processes. As recent studies
515 have again demonstrated, investigating the uncertainty in model structures, parameter estimation, and
516 observational testing data is crucial for advancing soil erosion modelling research (Benaud et al., 2021;
517 Eekhout et al., 2021; Schürz et al., 2020).

518 Importantly, while we demonstrated how conceptual models such as WaTEM/SEDEM can be useful for
519 understanding structural connectivity patterns, more dynamic and process-oriented models are necessary
520 for identifying so-called hot spots and hot moments of sediment connectivity (Owens, 2020; Turnbull
521 and Wainwright, 2019). In addition, WaTEM/SEDEM representations of sediment transfer could be
522 improved by incorporating the (dis)connectivity caused by linear features other than parcel borders and
523 grass buffer strips. This might entail assimilating the P_{Con} parameter to features such as roadside ditches

524 or terraces. Finally, mapping the location of hydraulic shortcuts within the road network, as well as the
525 extent to which these shortcuts increase the connectivity from hillslopes to water courses (e.g.,
526 Schönenberger and Stamm, 2021), should further improve sediment connectivity simulations in areas
527 such as the Baldegg catchment.

528 **5 Conclusions**

529 Here we employed a global sensitivity analysis of the WaTEM/SEDEM model to investigate the
530 influence of linear structures and landscape patchiness on sediment connectivity in the Baldegg
531 catchment. In particular, this novel application of WaTEM/SEDEM was implemented with the free
532 programming language R, and our code is available as supplementary material.

533 Our results demonstrated that assumptions about road connectivity were by far the most important factor
534 for modelling sediment transfer in the Baldegg catchment. Moreover, the comparison between extensive
535 model simulations and sediment rating curve calculations indicated that roads and hydraulic shortcuts
536 are likely to behave as conduits for sediment transport in the catchment. Hence, representing road
537 connectivity is crucial for modelling sediment transfer from hillslope to water courses in this agricultural
538 catchment of the Swiss Plateau, and potentially in other areas with a dense road drainage system.
539 Moreover, our results further highlighted the effects of linear structures and landscape patchiness on
540 sediment connectivity. These findings were made possible by the use of a model that was specifically
541 tailored to explore the particularities of our study area, by effectively exploring model assumptions and
542 the parameter space, and by the use of high-resolution spatial data.

543 Overall, we found that WaTEM/SEDEM was useful for investigating sediment connectivity in the
544 Baldegg catchment, as it allowed us to unravel some of the processes and structures regulating hillslope
545 sediment transport in the area. In the case the model is used for prediction and decision-making, we
546 recommend employing a fit-for-purpose rejectionist model testing framework, with multiple sources of
547 data, in order to evaluate the model's numerical accuracy and the quality of its spatial predictions.

548 **6 Code availability**

549 The code for the model simulations, sediment rating curves, and random forest analysis is available at
550 <https://doi.org/10.5281/zenodo.6560226>.

551 **7 Data availability**

552 The input data for the model simulations, the raw sediment concentration and discharge data, and
553 model results are available at <https://doi.org/10.5281/zenodo.6560226>.

554 **8 Author contributions**

555 PVGB and PF developed the model code, PVGB performed the simulations and analysed the data. SS
556 prepared model input data. PVGB prepared the manuscript with contributions from all authors. CA was
557 part of discussing ideas and revised the manuscript.

558 **9 Competing interests**

559 The authors declare no conflict of interest.

560 **10 Acknowledgements**

561 The authors would like to thank Robert Lovas, from the department of environment and energy of the
562 Canton of Lucerne, for supplying the sediment concentration and water discharge monitoring data, and
563 commenting on an earlier draft of this manuscript. We also appreciate the help from Axel Birkholz in
564 acquiring the data. PVGB would like to thank Franz Conen and Claudia Mignani for their multiple and
565 valuable inputs regarding the conceptualisation and preparation of this manuscript. We are thankful to
566 the comments from two anonymous reviewers, which greatly improved the quality of this manuscript.

567

568 **References**

- 569 Alder, S., Prasuhn, V., Liniger, H., Herweg, K., Hurni, H., Candinas, A. and Gujer, H. U.: A high-
570 resolution map of direct and indirect connectivity of erosion risk areas to surface waters in
571 Switzerland-A risk assessment tool for planning and policy-making, *Land use policy*, 48, 236–249,
572 doi:10.1016/j.landusepol.2015.06.001, 2015.
- 573 Antoniadis, A., Lambert-Lacroix, S. and Poggi, J. M.: Random forests for global sensitivity analysis:
574 A selective review, *Reliab. Eng. Syst. Saf.*, 206, 107312, doi:10.1016/j.ress.2020.107312, 2021.
- 575 von Arb, C., Stoll, S., Frossard, E., Stamm, C. and Prasuhn, V.: The time it takes to reduce soil legacy
576 phosphorus to a tolerable level for surface waters: What we learn from a case study in the catchment
577 of Lake Baldegg, Switzerland, *Geoderma*, 403, doi:10.1016/j.geoderma.2021.115257, 2021.
- 578 Baartman, J. E. M., Nunes, J. P., Masselink, R., Darboux, F., Biielders, C., Degré, A., Cantreul, V.,
579 Cerdan, O., Grangeon, T., Fiener, P., Wilken, F., Schindewolf, M. and Wainwright, J.: What do
580 models tell us about water and sediment connectivity?, *Geomorphology*, 367, 107300,
581 doi:10.1016/j.geomorph.2020.107300, 2020.
- 582 BAFU: Faktenblatt: Der Greifensee, Zustand bezüglich Wasserqualität, 1–8 [online] Available from:
583 <http://www.bafu.admin.ch>, 2016.
- 584 Bakker, M. M., Govers, G., van Doorn, A., Quetier, F., Chouvardas, D. and Rounsevell, M.: The
585 response of soil erosion and sediment export to land-use change in four areas of Europe: The
586 importance of landscape pattern, *Geomorphology*, 98(3–4), 213–226,
587 doi:10.1016/j.geomorph.2006.12.027, 2008.
- 588 Batista, P. V. G., Laceby, J. P., Davies, J., Carvalho, T. S., Tassinari, D., Silva, M. L. N., Curi, N. and
589 Quinton, J. N.: A framework for testing large-scale distributed soil erosion and sediment delivery
590 models : Dealing with uncertainty in models and the observational data, *Environ. Model. Softw.*, 137,
591 doi:10.1016/j.envsoft.2021.104961, 2021.
- 592 Bauer, M., Dostal, T., Krasa, J., Jachymova, B., David, V., Devaty, J., Strouhal, L. and Rosendorf, P.:
593 Risk to residents, infrastructure, and water bodies from flash floods and sediment transport, *Environ.*
594 *Monit. Assess.*, 191(2), doi:10.1007/s10661-019-7216-7, 2019.
- 595 Benaud, P., Anderson, K., Evans, M., Farrow, L., Glendell, M., James, M. R., Quine, T. A., Quinton,
596 J. N., Rickson, R. J. and Brazier, R. E.: Reproducibility, open science and progression in soil erosion
597 research. A reply to “Response to ‘National-scale geodata describe widespread accelerated soil
598 erosion’ Benaud et al. (2020) *Geoderma* 271, 114378” by Evans and Boardman (2021), *Geoderma*,
599 402, doi:10.1016/j.geoderma.2021.115181, 2021.

600 Bircher, P., Liniger, H. and Prasuhn, V.: Aktualisierung und Optimierung der Erosionsrisikokarte (
601 ERK2) Die neue ERK2 (2019) für das Ackerland der Schweiz, 2019.

602 Bispo, D. F. A., Batista, P.V.G., Guimarães, D. V., Silva, M. L. N., Curi, N. and Quinton, J. N.:
603 Monitoring land use impacts on sediment production : a case study of the pilot catchment from the
604 Brazilian program of payment for environmental services, *Rev. Bras. Ciência do Solo*, 44, :e0190167,
605 2020.

606 Boardman, J.: A 38-year record of muddy flooding at Breaky Bottom: Learning from a detailed case
607 study, *Catena*, 189(January), 104493, doi:10.1016/j.catena.2020.104493, 2020.

608 Borselli, L., Cassi, P. and Torri, D.: Prolegomena to sediment and flow connectivity in the landscape:
609 A GIS and field numerical assessment, *Catena*, 75(3), 268–277, doi:10.1016/j.catena.2008.07.006,
610 2008.

611 Breiman, L.: Random forests, *Machine Learning*, 45, 5-32, 2001.

612 Brenning, A., Bangs, D., Becker, M.: RSAGA: SAGA geoprocessing and terrain analysis. R package
613 version 1.3.0., 2018.

614 Calsamiglia, A., García-Comendador, J., Fortesa, J., López-Tarazón, J. A., Crema, S., Cavalli, M.,
615 Calvo-Cases, A. and Estrany, J.: Effects of agricultural drainage systems on sediment connectivity in a
616 small Mediterranean lowland catchment, *Geomorphology*, 318, 162–171,
617 doi:10.1016/j.geomorph.2018.06.011, 2018a.

618 Calsamiglia, A., Fortesa, J., García-Comendador, J., Lucas-Borja, M. E., Calvo-Cases, A. and Estrany,
619 J.: Spatial patterns of sediment connectivity in terraced lands: Anthropogenic controls of catchment
620 sensitivity, *L. Degrad. Dev.*, 29(4), 1198–1210, doi:10.1002/ldr.2840, 2018b.

621 Cavalli, M., Trevisani, S., Comiti, F. and Marchi, L.: Geomorphometric assessment of spatial
622 sediment connectivity in small Alpine catchments, *Geomorphology*, 188, 31–41,
623 doi:10.1016/j.geomorph.2012.05.007, 2013.

624 Chartin, C., Evrard, O., Salvador-Blanes, S., Hirschberger, F., Van Oost, K., Lefèvre, I., Daroussin, J.
625 and Macaire, J. J.: Quantifying and modelling the impact of land consolidation and field borders on
626 soil redistribution in agricultural landscapes (1954-2009), *Catena*, 110, 184–195,
627 doi:10.1016/j.catena.2013.06.006, 2013.

628 Cohn, T. A., Caulder, D. L., Gilroy, J., Zynjuk, L. D. and Summers, R. M.: The Validity of a Simple
629 Statistical Model for Estimating, *Water Resour. Res.*, 28(9), 2353–2363, 1992.

630 Conrad, O., Bechtel, B., Bock, M., Dietrich, H., Fischer, E., Gerlitz, L., Wehberg, J., Wichmann, V.
631 and Böhner, J.: System for Automated Geoscientific Analyses (SAGA) v.2.2.2, 1991–2007,
632 doi:10.5194/gmd-8-1991-2015, 2015.

633 Croke, J., Mockler, S., Fogarty, P. and Takken, I.: Sediment concentration changes in runoff pathways
634 from a forest road network and the resultant spatial pattern of catchment connectivity,
635 *Geomorphology*, 68(3–4), 257–268, doi:10.1016/j.geomorph.2004.11.020, 2005.

636 Desmet, P., Govers, G.: A GIS procedure for automatically calculating the USLE LS factor on
637 topographically complex landscape units, *J. Soil Water Conserv.*, 51, 427–433, 1996.

638 Eekhout, J. P. C., Millares-Valenzuela, A., Martínez-Salvador, A., García-Lorenzo, R., Pérez-Cutillas,
639 P., Conesa-García, C. and de Vente, J.: A process-based soil erosion model ensemble to assess model
640 uncertainty in climate-change impact assessments, *L. Degrad. Dev.*, 32, 2409–2422,
641 doi:10.1002/ldr.3920, 2021.

642 Evrard, O., Cerdan, O., van Wesemael, B., Chauvet, M., Le Bissonnais, Y., Raclot, D., Vandaele, K.,
643 Andrieux, P. and Bielders, C.: Reliability of an expert-based runoff and erosion model: Application of
644 STREAM to different environments, *Catena*, 78(2), 129–141, doi:10.1016/j.catena.2009.03.009, 2009.

645 Fiener, P. and Auerswald, K.: Measurement and modeling of concentrated runoff in grassed
646 waterways, *J. Hydrol.*, 301(1–4), 198–215, doi:10.1016/j.jhydrol.2004.06.030, 2005.

647 Fiener, P., Auerswald, K. and Van Oost, K.: Spatio-temporal patterns in land use and management
648 affecting surface runoff response of agricultural catchments-A review, *Earth-Science Rev.*, 106(1–2),
649 92–104, doi:10.1016/j.earscirev.2011.01.004, 2011.

650 Fiener, P., Wilken, F. and Auerswald, K.: Filling the gap between plot and landscape scale – eight
651 years of soil erosion monitoring in 14 adjacent watersheds under soil conservation at Scheyern,
652 Southern Germany, *Adv. Geosci. Discuss.*, (July), doi:adgeo-2019-4, 2019.

653 Fryirs, K.: (Dis)Connectivity in catchment sediment cascades: A fresh look at the sediment delivery
654 problem, *Earth Surf. Process. Landforms*, 38(1), 30–46, doi:10.1002/esp.3242, 2013.

655 Gelman, A. and Hill, J.: *Data Analysis Using Regression and Multilevel/Hierarchical Models*,
656 Cambridge University Press, New York., R package version 1.12.2, 2007.

657 Govers, G.: Misapplications and misconceptions of erosion models, in: *Handbook of erosion*
658 *modelling*, edited by: Morgan, R. P. C., Nearing, M.A., Blackwell Publishing Ltd., Chichester, United
659 Kingdom, 117–134, 2011.

660 Heckmann, T., Cavalli, M., Cerdan, O., Foerster, S., Javaux, M., Lode, E., Smetanová, A., Vericat, D.
661 and Brardinoni, F.: Indices of sediment connectivity: opportunities, challenges and limitations, *Earth-*
662 *Science Rev.*, 187(December 2017), 77–108, doi:10.1016/j.earscirev.2018.08.004, 2018.

663 IUSS Working Group WRB. *World Reference Base for Soil Resources; IUSS Working Group WRB:*
664 *Wageningen, The Netherlands, 2006; pp. 1–128.*

665 Keller, B.: Lake Lucerne and its spectacular landscape, in: *Landscapes and landforms of Switzerland*,
666 edited by Reynard, E., Springer Nature Switzerland, Cham, Switzerland, 305-324, 2021.

667 Krasa, J., Dostal, T., Jachymova, B., Bauer, M. and Devaty, J.: Soil erosion as a source of sediment
668 and phosphorus in rivers and reservoirs – Watershed analyses using WaTEM/SEDEM, *Environ. Res.*,
669 171(January), 470–483, doi:10.1016/j.envres.2019.01.044, 2019.

670 Kupferschmied, P.: CP-Tool: Ein Programm zur Berechnung des Fruchtfolge- und
671 Bewirtschaftungsfaktors (CP-Faktor) der Allgemeinen Bodenabtragsgleichung (ABAG), 2019.

672 Laceby, J. P., Batista, P. V. G., Taube, N., Kruk, M. K., Chung, C., Evrard, O. and Orwin, J. F.:
673 Tracing total and dissolved material in a western Canadian basin using quality control samples to
674 guide the selection of fingerprinting parameters for modelling, *Catena*, 200(April 2020), 105095,
675 doi:10.1016/j.catena.2020.105095, 2021.

676 Lacoste, M., Michot, D., Viaud, V., Evrard, O. and Walter, C.: Combining ¹³⁷Cs measurements and a
677 spatially distributed erosion model to assess soil redistribution in a hedgerow landscape in
678 northwestern France (1960-2010), *Catena*, 119, 78–89, doi:10.1016/j.catena.2014.03.004, 2014.

679 Lavrieux, M., Birkholz, A., Meusburger, K., Wiesenberg, G. L. B., Gilli, A., Stamm, C. and Alewell,
680 C.: Plants or bacteria? 130 years of mixed imprints in Lake Baldegg sediments (Switzerland), as
681 revealed by compound-specific isotope analysis (CSIA) and biomarker analysis, *Biogeosciences*,
682 16(10), 2131–2146, doi:10.5194/bg-16-2131-2019, 2019.

683 Ledermann, T., Herweg, K., Liniger, H. P., Schneider, F., Hurni, H. and Prasuhn, V.: Applying
684 erosion damage mapping to assess and quantify off-site effects of soil erosion in Switzerland, *L.*
685 *Degrad. Dev.*, 21, 353–366, 2010.

686 Liaw, A., Wiener, M.: Classification and regression by randomForest. *R News*, 2, 18–22, R package
687 version 4.7.1, 2002.

688 Mahoney, D. T., Fox, J. F. and Al-Aamery, N.: Watershed erosion modeling using the probability of
689 sediment connectivity in a gently rolling system, *J. Hydrol.*, 561(April), 862–883,
690 doi:10.1016/j.jhydrol.2018.04.034, 2018.

691 Mahoney, D. T., Fox, J., Al-Aamery, N. and Clare, E.: Integrating connectivity theory within
692 watershed modelling part I: Model formulation and investigating the timing of sediment connectivity,
693 *Sci. Total Environ.*, 740, 140385, doi:10.1016/j.scitotenv.2020.140385, 2020a.

694 Mahoney, D. T., Fox, J., Al-Aamery, N. and Clare, E.: Integrating connectivity theory within
695 watershed modelling part II: Application and evaluating structural and functional connectivity, *Sci.*
696 *Total Environ.*, 740, 140386, doi:10.1016/j.scitotenv.2020.140386, 2020b.

697 MeteoSwiss. SwissMetNet Surface Weather Stations, Mosen MOA, 2010-2019 (Switzerland), 2021.

698 Müller, B., Gächter, R. and Wüest, A.: Accelerated water quality improvement during
699 oligotrophication in peri-alpine lakes, *Environ. Sci. Technol.*, 48(12), 6671–6677,
700 doi:10.1021/es4040304, 2014.

701 Notebaert, B., Vaes, B., Govers, G., Van Oost, K., Van Rompaey, A., and Verstraeten, G.: WaTEM /
702 SEDEM version 2006 Manual., 2006.

703 Nunes, J. P., Wainwright, J., Biielders, C. L., Darboux, F., Fiener, P., Finger, D. and Turnbull, L.:
704 Better models are more effectively connected models, *Earth Surf. Process. Landforms*, 43(6), 1355–
705 1360, doi:10.1002/esp.4323, 2018.

706 Owens, P. N.: Soil erosion and sediment dynamics in the Anthropocene: a review of human impacts
707 during a period of rapid global environmental change, *J. Soils Sediments*, 20(12), 4115–4143,
708 doi:10.1007/s11368-020-02815-9, 2020.

709 Parsons, A. J., Wainwright, J., Brazier, R. E. and Powell, D. M.: Is sediment delivery a fallacy? Reply,
710 *Earth Surf. Process. Landforms*, 34(February), 155–161, doi:10.1002/esp, 2009.

711 Persichillo, M. G., Bordoni, M., Cavalli, M., Crema, S. and Meisina, C.: The role of human activities
712 on sediment connectivity of shallow landslides, *Catena*, 160(August 2016), 261–274,
713 doi:10.1016/j.catena.2017.09.025, 2018.

714 Pianosi, F., Beven, K., Freer, J., Hall, J. W., Rougier, J., Stephenson, D. B. and Wagener, T.:
715 Sensitivity analysis of environmental models: A systematic review with practical workflow, *Environ.*
716 *Model. Softw.*, 79, 214–232, doi:10.1016/j.envsoft.2016.02.008, 2016.

717 Pfiffner, O. A.: The structural landscapes of Central Switzerland, in: *Landscapes and landforms of*
718 *Switzerland*, edited by Reynard, E., Springer Nature Switzerland, Cham, Switzerland, 159-172, 2021.

719 Prasuhn, V.: Twenty years of soil erosion on-farm measurement: annual variation, spatial distribution
720 and the impact of conservation programmes for soil loss rates in Switzerland, *Earth Surf. Process.*
721 *Landforms*, doi:10.1002/esp.4829, 2020.

722 Remund, D., Liebisch, F., Liniger, H. P., Heinimann, A. and Prasuhn, V.: The origin of sediment and
723 particulate phosphorus inputs into water bodies in the Swiss Midlands – A twenty-year field study of
724 soil erosion, *Catena*, 203(March), 105290, doi:10.1016/j.catena.2021.105290, 2021.

725 Renard, K., Foster, G. R., Weesies, G. A., McCool, D. K. and Yoder, D. C.: *Predicting Soil Erosion by*
726 *Water: A Guide to Conservation Planning With the Revised Universal Soil Loss Equation (RUSLE)*,
727 1997.

728 R Core Team. R: A language for statistical computing. R Foundation for Statistical Computing,
729 Vienna, Austria. URL <https://www.R-project.org>, 2021.

730 Saggau, P., Kuhwald, M. and Duttmann, R.: Integrating soil compaction impacts of tramlines into soil
731 erosion modelling: A field-scale approach, *Soil Syst.*, 3(3), 1–28, doi:10.3390/soilsystems3030051,
732 2019.

733 Schmidt, S., Alewell, C., Panagos, P. and Meusburger, K.: Regionalization of monthly rainfall
734 erosivity patterns in Switzerland, *Hydrol. Earth Syst. Sci.*, 20(10), 4359–4373, doi:10.5194/hess-20-
735 4359-2016, 2016.

736 Schmidt, S., Ballabio, C., Alewell, C., Panagos, P. and Meusburger, K.: Filling the European blank
737 spot—Swiss soil erodibility assessment with topsoil samples, *J. Plant Nutr. Soil Sci.*, 181(5), 737–748,
738 doi:10.1002/jpln.201800128, 2018a.

739 Schmidt, S., Alewell, C. and Meusburger, K.: Mapping spatio-temporal dynamics of the cover and
740 management factor (C-factor) for grasslands in Switzerland, *Remote Sens. Environ.*, 211(April), 89–
741 104, doi:10.1016/j.rse.2018.04.008, 2018b.

742 Schönenberger, U. and Stamm, C.: Hydraulic shortcuts increase the connectivity of arable land areas
743 to surface waters, *Hydrol. Earth Syst. Sci.*, 25(4), 1727–1746, doi:10.5194/hess-25-1727-2021, 2021.

744 Schürz, C., Mehdi, B., Kiesel, J., Schulz, K. and Herrnegger, M.: A systematic assessment of
745 uncertainties in large-scale soil loss estimation from different representations of USLE input factors—a
746 case study for Kenya and Uganda, *Hydrol. Earth Syst. Sci.*, 24(9), 4463–4489, doi:10.5194/hess-24-
747 4463-2020, 2020.

748 Sherriff, S. C., Rowan, J. S., Fenton, O., Jordan, P., Melland, A. R., Mellander, P. E. and Huallacháin,
749 D.: Storm Event Suspended Sediment-Discharge Hysteresis and Controls in Agricultural Watersheds:
750 Implications for Watershed Scale Sediment Management, *Environ. Sci. Technol.*, 50(4), 1769–1778,
751 doi:10.1021/acs.est.5b04573, 2016.

752 Starkloff, T. and Stolte, J.: Applied comparison of the erosion risk models EROSION 3D and LISEM
753 for a small catchment in Norway, *Catena*, 118, 154–167, doi:10.1016/j.catena.2014.02.004, 2014.

754 Stenfert Kroese, J., Batista, P. V. G., Jacobs, S. R., Breuer, L., Quinton, J. N. and Rufino, M. C.:
755 Agricultural land is the main source of stream sediments after conversion of an African montane
756 forest, *Sci. Rep.*, 10(1), 1–15, doi:10.1038/s41598-020-71924-9, 2020.

757 Stoll, S., Arb, C. von, Jorg, C., Kopp, S. and Prasuhn, V.: Evaluation der stark zur Phosphor-Belastung
758 des Baldeggersees beitragenden Flächen., 2019.

759 Swisstopo. SwissALTI3D. Das hoch aufgelöste Terrainmodell der Schweiz, 2014a.

760 Swisstopo. Swissimage. Das digitale Farbborthophotomosaik der Schweiz. 2014b.

761 Swisstopo. Swiss Map Vector 25 Beta, Das digitale Landschaftsmodell der Schweiz. 2018.

762 Swisstopo. SwissTLM3D. Das grossmassstäbliche Topografische Landschaftsmodell der Schweiz,
763 2020.

764 Teranes, J. L. and Bernasconi, S. M.: Factors controlling $\delta^{13}\text{C}$ values of sedimentary carbon in
765 hypertrophic Baldeggersee, Switzerland, and implications for interpreting isotope excursions in lake
766 sedimentary records, *Limnol. Oceanogr.*, 50(3), 914–922, doi:10.4319/lo.2005.50.3.0914, 2005.

767 Turnbull, L. and Wainwright, J.: From structure to function: Understanding shrub encroachment in
768 drylands using hydrological and sediment connectivity, *Ecol. Indic.*, 98(November 2018), 608–618,
769 doi:10.1016/j.ecolind.2018.11.039, 2019.

770 Van Oost, K., Govers, G. and Desmet, P. J. J.: Evaluating the effects of changes in landscape structure
771 on soil erosion by water and tillage, *Landsc. Ecol.*, 15(6), 577–589, doi:10.1023/A:1008198215674,
772 2000.

773 Van Rompaey, A., Verstraeten, G., Van Oost, K., Govers, G. and Poesen, J.: Modelling mean annual
774 sediment yield using a distributed approach, *Earth Surf. Process. Landforms*, 26(11), 1221–1236,
775 doi:10.1002/esp.275, 2001.

776 Verstraeten, G., Van Oost, K., Van Rompaey, A. J. J., Poesen, J. and Govers, G.: Evaluating an
777 integrated approach to catchment management to reduce soil loss and sediment pollution through
778 modelling, *Soil Use Manag.*, 18(4), 386–394, doi:10.1111/j.1475-2743.2002.tb00257.x, 2010.

779 Vigiak, O. and Bende-Michl, U.: Estimating bootstrap and Bayesian prediction intervals for
780 constituent load rating curves, *Water Resour. Res.*, 49(12), 8565–8578, doi:10.1002/2013WR013559,
781 2013.

782 Wainwright, J., Turnbull, L., Ibrahim, T. G., Lexartza-Artza, I., Thornton, S. F. and Brazier, R. E.:
783 Linking environmental regimes, space and time: Interpretations of structural and functional
784 connectivity, *Geomorphology*, 126(3–4), 387–404, doi:10.1016/j.geomorph.2010.07.027, 2011.

785 Wehrli, B., Lotter, A. F., Schaller, T. and Sturm, M.: High-resolution varve studies in Baldeggersee
786 (Switzerland): Project overview and limnological background data, *Aquat. Sci.*, 59(4), 285–294,
787 doi:10.1007/BF02522359, 1997.

788 Wilken, F., Fiener, P. and Van Oost, K.: Modelling a century of soil redistribution processes and
789 carbon delivery from small watersheds using a multi-class sediment transport model, *Earth Surf. Dyn.*,
790 5, 113–124, doi:10.5194/esurf-5-113-2017, 2017.

791